APPLICATION TO THE VIGGEN AIRCRAFT CONFIGURATION OF THE POLAR COORDINATE METHOD FOR UNSTEADY SUBSONIC FLOW

Valter J. E. Stark

Saab-Scania AB, Linköping, Sweden

Abstract

A Fortran program for calculation of aerodynamic forces on oscillating wing configurations in subsonic flow has been developed on the basis of the so called Polar Coordinate Method. In this method, the normal velocities, that correspond to the functions in a linear approximation to the jump in the advanced velocity potential, are calculated by using polar coordinates as integration variables and a tangent function for subtraction of the kernel function singularity. The program which is applicable to configurations with control-surfaces has been applied to the Viggen configuration. Results from this application are shown in the paper together with favourable comparisons with reliable results of other methods for three simple wings.

Symbols

A	aspect ratio
$A_{p,q}$	aerodynamic coefficients
B	$1-M^2$
C_L	lift coefficient
C_M	pitching moment coefficient
H_p^n	shape function for the p^{th} mode and the surface S_n
L	reference length, specified in examples
M	Mach number
p	$p'/(\frac{1}{2}\rho U^2)$, normalized pressure
$\Delta p(u,v)$	difference between values of p on the two sides of S_n
S	reference area, specified in examples
U	free-stream velocity
x^n, y^n, z^n	local coordinates for S_n, normalized and referred to L
$D_{i,n}$, $S_{i,n}$, $Z_{i,n}$	arbitrary parameters determining P_i, i = 1, 2, ... 5, in Eq. (40) and (41)
ρ	free-stream density
$\Delta\phi(u,v)$	difference between values of the advanced velocity potential on the two sides of S_n
μ_S, ν_S	numbers of chordwise and spanwise factors in approximations to $\Delta\phi(u,v)$
ω	$\omega'/(U/L)$, normalized circular frequency
β	$\sqrt{B}$, the Prandtl-Glauert factor

Introduction

In oscillating-surface theory, the oscillating wing is replaced by a thin planar surface. In analogy with this theory, we assume here that a complete aircraft or a general wing configuration may be replaced by a number of thin planar surfaces. These are chosen as trapezoids. The pressure jump that results across the trapezoids due to the harmonic oscillation can be obtained from a linear approximation to the jump in the advanced velocity potential and this approximation can be determined on the basis of the condition for the normal velocity. This implies that the normal velocities that correspond to the functions in the approximation have to be calculated. In the Polar Coordinate Method which will here be described and applied, this calculation is made by using polar coordinates as integration variables.

The Polar Coordinate Method which has earlier been applied to planar wings in Ref. 1 and to wing configurations in Ref. 2 also employs a tangent plane to part of the integrand for subtraction of the kernel function singularity. This procedure which was studied in Ref. 3 gives rise to two integrals one of which can be evaluated in closed form and the other numerically.

The Fortran program that was employed in Ref. 2 has been improved by using polar integration variables in all integrals and not only in those for which the integration region contains the control point projection. As the Viggen configuration makes great demands on the method that is used, the improved program has been applied to this configuration. We show here some of the results and present in addition a few comparisons with certain reliable values from other methods[6] for simple wings.

The investigation shows that the computer program developed is capable of producing accurate results and that it is more economic than the Fortran program that was first developed on the basis of the Lifting Line Element Method[4].

Preliminaries

We consider an idealized configuration consisting of thin planar trapezoidal surfaces whose parallel sides are directed in the free-stream direction. The shape and orientation of the n^{th} surface which is denoted by S_n, n = 1, 2, ... n_S, is uniquely defined by the position vectors of its corners. These vectors which may be given in terms of components in a basic coordinate system form input data to the computer program developed.

In addition to the basic system, we use a local coordinate system for each trapezoidal surface. The coordinates of an arbitrary point in the local system for S_n are denoted x^n, y^n, z^n. The x^n-axis and the z^n-axis shall be directed in the free-stream direction and in the positive normal direction respectively, the origin shall lie at the center of the inboard chord, and the y^n-axis shall point to the outboard chord.

The positive normal direction and the inboard and outboard chords are defined by the order in which the input data for the position vectors of the corners are given. We prescribe the following order: downstream corner at outboard chord, up-

stream corner at outboard chord, upstream corner at inboard chord, and finally downstream corner at inboard chord. The positive normal direction is defined as the direction of advancement of a right-handed screw when rotated in agreement with the order mentioned. If S_n is joined to another surface only along one of the side edges, the other free side edge shall be regarded as the outboard chord.

It is understood that all quantities in the sequel are dimensionless quantities unless otherwise specified. The coordinates x^n, y^n, z^n and all other lengths are referred to some typical length L, velocities to the free-stream velocity U, and potentials to UL. The perturbation pressure p is referred to the free-stream dynamic pressure $\frac{1}{2}\rho U^2$ and the reduced circular frequency ω is referred to U/L.

We use the so called advanced velocity potential, the advanced pressure, and the advanced normal velocity. In the harmonic case which is here considered, these quantities which have previously been introduced[5] are defined as the products of the ordinary quantities and the factor $\exp(i\omega(x^n-x_1^n))$; x_1^n being the x^n-coordinate of the origin of the local coordinate system for S_1.

The quantities, that shall be calculated, include in the first place the generalized aerodynamic coefficients $A_{p,q}$. These are defined as follows. Consider a given dimensionless shape function $H_q^n(x^n,y^n)$ and let the configuration oscillate with an amplitude equal to $LH_q^n(x^n,y^n)$ in the normal direction of S_n. Due to the oscillation there appears a perturbation pressure $p_q(x^n,y^n,z^n)$ in the flow and a pressure jump across S_n. This jump is defined as

$$\Delta p_q^n(x^n,y^n) = p_q(x^n,y^n,0+) - p_q(x^n,y^n,0-) \qquad (1)$$

and is related to the jump $\Delta\underline{\phi}_q(x^n,y^n)$ in the advanced velocity potential by

$$\Delta p_q^n(u,v) = -2e^{-i\omega(u-x_1^n)}\Delta\underline{\phi}_{qu}(u,v) \qquad (2)$$

where the subscript u indicates differentiation with respect to u. The aerodynamic coefficients are defined by the formula

$$A_{p,q} = \frac{L^2}{S}\sum_{n=1}^{n_S}\iint_{S_n} H_p^n(u,v)\,\Delta p_q^n(u,v)\,dudv \qquad (3)$$

which can also be written in the form

$$A_{p,q} = \frac{-2L^2}{S}\sum_{n=1}^{n_S}\iint_{S_n} H_p^n(u,v)e^{-i\omega(u-x_1^n)}\Delta\underline{\phi}_{qu}(u,v)\,dudv \qquad (4)$$

If the first two shape functions define rigid translation and pitch with amplitudes L and one radian and if the reference area S and the reference length L are the same as the reference quantities used for the ordinary coefficients C_L and C_M, the coefficients $A_{1,q}$ and $A_{2,q}$ are equivalent with C_L and C_M.

The numerical procedure that has been developed is based on a linear approximation to the jump in the advanced velocity potential. In order to satisfy the condition for the normal velocity it is required to calculate the normal velocities that correspond to the functions in this approximation at suitably located control points. The calculation of these velocities is the main task that will be considered in the sequel.

Theory for calculation of the normal velocity matrix

The advanced velocity potential $\underline{\phi}(\underline{x}^m) = \underline{\phi}(x^m, y^m, z^m)$ at a point with coordinates x^m, y^m, z^m in the local coordinate system for S_m may be expressed in the form

$$\underline{\phi}(\underline{x}^m) = \sum_{n=1}^{n_S} -\iint_{S_n+W_n}\frac{\partial}{\partial z^n}(4\pi R e^{i\omega\tau})^{-1}\Delta\underline{\phi}(u,v)\,dudv \qquad (5)$$

where $\tau = (u-x^n+MR)/B$, $R = (\rho^2+B(z^n)^2)^{\frac{1}{2}}$, $\rho = ((u-x^n)^2+B(v-y^n)^2)^{\frac{1}{2}}$, and $B = 1-M^2$. M is the Mach number, n_S the number of surfaces, and $\Delta\underline{\phi}(u,v)$ the jump in the advanced potential across S_n.

The integration region consists of the trapezoidal surface S_n and its wake, but the latter region may be replaced by a finite area, for the contribution from the distant part of the wake is small and negligible. In the sequel, the symbol W_n therefore denotes a cropped wake. Usually it is satisfactory to cut off the wake at a distance equal to $4\beta s$ from the downstream end of the configuration; s being the semispan and $\beta = \sqrt{B}$ the Prandtl-Glauert factor.

For a given advanced potential jump across each of the surfaces, the relation (5) defines the corresponding advanced potential. It also defines integral expressions for the advanced velocity components which can be obtained by differentiation. The component W^m in the normal direction of S_m which we are interested in is obtained by differentiating the integrals in the sum (5) with respect to z^m.

A numerical procedure for calculation of W^m has been developed by using polar coordinates as integration variables. This approach, which has been described in two earlier papers[1,5] is favorable, for the strong variation of the known integrand part occurs exclusively with the radial variable ρ while the variation with the angular variable θ is slight. The polar variables are defined by the relations $u-x^n = \rho\cos\theta$ and $\beta(v-y^n) = \rho\sin\theta$.

The differentiation and the introduction of the polar variables results in the following formulas:

$$W^m = \sum_{n=1}^{n_S} W^{m,n} \qquad (6)$$

$$W^{m,n} = \iint_{S_n+W_n} F(\rho,\theta)\,d\rho\,d\theta \qquad (7)$$

$$F(\rho,\theta) = \left(G\frac{\partial y^n}{\partial z^m} + H\frac{\partial z^n}{\partial z^m}\right)\frac{e^{-i\omega\tau}}{4\pi R^5}\beta\rho\Delta\underline{\phi}(u,v) \qquad (8)$$

$$G = -\beta z^n\rho(3-Q^2+3iQ)\sin\theta \qquad (9)$$

$$H = -B(Qz^n)^2 + (1+iQ)(-\rho^2+2B(z^n)^2) \qquad (10)$$

$$Q = \omega MR/B \qquad (11)$$

$$R = (\rho^2 + B(z^n)^2)^{\frac{1}{2}} \tag{12}$$

$$\tau = (\rho \cos\theta + MR)/B \tag{13}$$

The integral (7) may be evaluated by first integrating in the radial direction. The inner integral will then be a function of θ. Due to the corners of the integration region S_n+W_n, this function exhibits irregularities at the values of θ that correspond to rays through the corners. The outer integral in θ is therefore computed as a sum of subintegrals over the intervals between the irregularities. Thus we write

$$W^{m,n} = \sum_{r=1}^{r_S} \int_{\theta_I}^{\theta_S} d\theta \int_{\rho_I}^{\rho_S} F(\rho,\theta)\,d\rho \tag{14}$$

where θ_I and θ_S denote the values of θ at the ends of the r^{th} subinterval. The limit ρ_S is the value of ρ at the distant edge while ρ_I is the value at the near edge.

The number of subintegrals r_S, the interpretation of the subintegrals, and the method employed for evaluation of these depend on the location of the control point $\underline{x}^n$. In particular we must distinguish between the case in which the projection (x^n,y^n) of the control point on the plane $z^n = 0$ lies within S_n+W_n and the case in which the projection lies outside this area. The limit ρ_I is zero in the former case.

If the projection lies outside S_n+W_n, the integral for $W_{m,n}$ is calculated as a sum of three subintegrals. The corresponding subregions which are formed by rays through the corners of S_n+W_n are shown in Fig. 1 . They consist of one quadrilateral and two triangles. The subintegrals are calculated by a numerical routine that has been written for the quadrilateral and is applied to all three regions. This is possible since the triangles are special quadrilaterals.

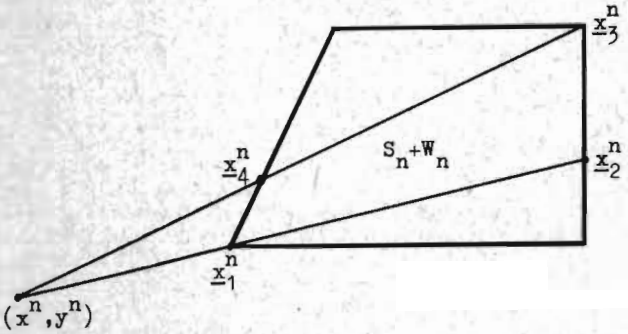

FIG. 1 DIVISION OF $S_n + W_n$

As can be seen from the figure, one has to calculate position vectors for two intersections between two rays and two edges of S_n+W_n which can be done by a simple formula. The formula demands, however, appropriate input data which depend on the location of (x^n,y^n). For each corner of S_n+W_n there are three sets of data which correspond to three areas within which (x^n,y^n) can lie. These areas are bounded by the extensions of the edges and the diagonals of S_n+W_n.

The numerical quadrature routine first transforms the position vectors $\underline{x}_1^n$, $\underline{x}_2^n$, $\underline{x}_3^n$, $\underline{x}_4^n$, and $\underline{x}^n$ for the corners of the quadrilateral and the control point into new vectors. The new vectors which are denoted by $\bar{\underline{x}}_1^n$, $\bar{\underline{x}}_2^n$, $\bar{\underline{x}}_3^n$, $\bar{\underline{x}}_4^n$, and $\bar{\underline{x}}^n$ are obtained by multiplying the components in the y^n-direction by β. The quadrilateral corresponding to the new vectors which define the integration limits ρ_I, ρ_S, θ_I, and θ_S is shown in Fig. 2.

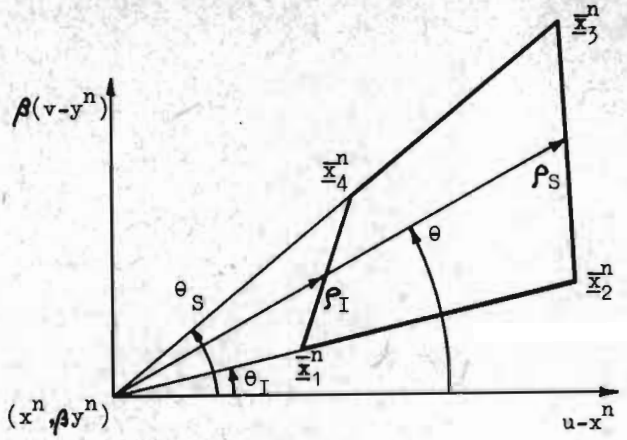

FIG. 2 INTEGRATION LIMITS FOR SUBINTEGRALS

The integrand of the inner integral may be irregular at the limits ρ_I and ρ_S. The variable ρ is therefore changed. We define a new variable of integration s by the relation

$$\rho = \rho_I + (\rho_S-\rho_I)(3s^2-2s^3) \tag{15}$$

which effects a stretching at the ends of the interval. By further putting

$$\theta = \theta_I + (\theta_S-\theta_I)t \tag{16}$$

the relation (14) assumes the form

$$W^{m,n} = \sum_{r=1}^{r_S} (\theta_S-\theta_I)\int_0^1 6(\rho_S-\rho_I)dt \int_0^1 F(\rho,\theta)(1-s)s\,ds\,ds \tag{17}$$

The integrals in this expression are evaluated by numerical quadrature. This is performed by dividing the normalized integration intervals into subintervals of equal length and by applying the Gaussian formula with 2 integration points in each subinterval. Thereby we obtain the formula

$$W^{m,n} \approx \sum_{r=1}^{r_S} \frac{\theta_S-\theta_I}{2j_S} \sum_{j=1}^{2j_S} \frac{6(\rho_S-\rho_I)}{2i_S} \sum_{i=1}^{2i_S} F(\rho,\theta)(1-s)s \tag{18}$$

where

$$\theta = \theta_I + (\theta_S-\theta_I)t \tag{19}$$

$$t = \begin{cases} (j - 1/\sqrt{3})/(2j_S) & j \text{ odd} \\ (j-1+1/\sqrt{3})/(2j_S) & j \text{ even} \end{cases} \tag{20}$$

$$\rho = \rho_I + (\rho_S-\rho_I)(3s^2-2s^3) \tag{21}$$

and

$$s = \begin{cases} (i - 1/\sqrt{3})/(2i_S) & i \text{ odd} \\ (i-1+1/\sqrt{3})/(2i_S) & i \text{ even} \end{cases} \tag{22}$$

The subinterval numbers i_S and j_S may be determined in a way that will be described in the sequel.

If the projection (x^n,y^n) lies within S_n+W_n, we must distinguish between two subcases. These subcases which correspond to $z^n \neq 0$ and $z^n = 0$ must be treated in different ways.

The subcase $z^n \neq 0$ involves no difficulty, for the numerical procedure that was described above can be used also in this case. The behaviour of the integrand at the trailing edge makes it desirable, however, to calculate the integral as a sum of separate integrals over S_n and W_n. For this reason and as the projection can lie either on S_n or on W_n we get two subdivisions. These are shown in Fig. 3. The formula (18) can be applied to each of the two subdivisions which contain 7 subareas. Hence, $r_S = 7$.

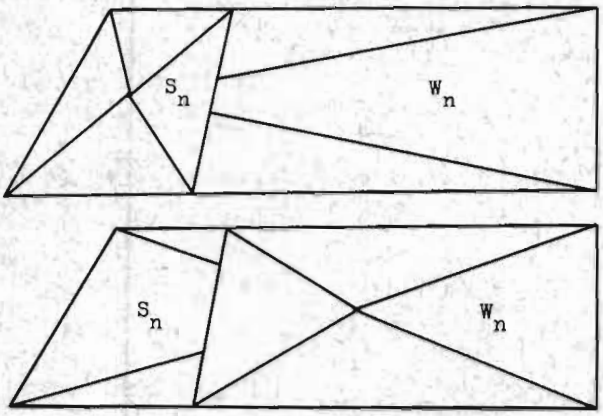

FIG. 3 SUBDIVISIONS FOR THE CASE IN WHICH THE CONTROL POINT PROJECTION LIES WITHIN S_n OR W_n

The subcase $z^n = 0$ represents a difficult problem, for it requires that the limit of the integral (7) for z^n approaching zero shall be calculated.

We use for this purpose the tangent plane concept which was introduced in Ref. 3 . This implies that a linear function which defines a tangent plane to part of the integrand is subtracted from the integrand part. In an earlier investigation[1] we used a so called tangent function instead of the tangent plane, but the tangent plane yields a slightly simpler and equally efficient procedure.

The integrand part considered consists of the product $\beta(1+iQ)e^{-i\omega\tau}\Delta\bar{\phi}(u,v)$. By expanding this product about the point $(x^n,y^n,0)$ and by neglecting second order terms and terms of higher order we obtain

$$\beta(1+iQ)e^{-i\omega\tau}\Delta\bar{\phi}(u,v) \approx \beta(1+iQ)\Big[\,1 - i\omega(u-x^n)/B - iQ\Big]\Big[\Delta\bar{\phi} + \Delta\bar{\phi}_x(u-x^n) + \Delta\bar{\phi}_y(v-y^n)\Big] \approx$$

$$\beta\Big[1 - i\omega(u-x^n)/B\Big]\Big[\Delta\bar{\phi} + \Delta\bar{\phi}_x(u-x^n) + \Delta\bar{\phi}_y(v-y^n)\Big] \approx$$

$$\beta\Delta\bar{\phi} + (\beta\Delta\bar{\phi}_x - \frac{i\omega}{\beta}\Delta\bar{\phi})(u-x^n) + \Delta\bar{\phi}_y\beta(v-y^n) =$$

$$= \beta\Delta\bar{\phi} + \Big[(\beta\Delta\bar{\phi}_x - \frac{i\omega}{\beta}\Delta\bar{\phi})\cos\theta + \Delta\bar{\phi}_y\sin\theta\Big]\rho \qquad (23)$$

where

$$\Delta\bar{\phi} = \Delta\bar{\phi}(x^n,y^n) \qquad (24)$$

$$\Delta\bar{\phi}_x = \frac{\partial}{\partial x^n}\Delta\bar{\phi}(x^n,y^n) \qquad (25)$$

$$\Delta\bar{\phi}_y = \frac{\partial}{\partial y^n}\Delta\bar{\phi}(x^n,y^n) \qquad (26)$$

The final expression in the right hand member defines the tangent plane to the integrand part at the point $(u,v) = (x^n,y^n)$. Subtracting the tangent plane from the integrand part and compensating this by addition of the same function, we get an expression for $W^{m,n}$ which may be written as

$$W^{m,n} = E + S \qquad (27)$$

The term S in this formula is the limit of that integral, that contains the difference between the integrand part and the tangent plane. The integrand of this integral remains regular at the point $(u,v) = (x^n,y^n)$ when z^n assumes the value zero, and so the limit of the integral can be obtained by integrating the limit of the integrand. The limit of the integrand reads

$$F(\rho,\theta) = \Big[\beta\Delta\bar{\phi} + ((\beta\Delta\bar{\phi}_x - \frac{i\omega}{\beta}\Delta\bar{\phi})\cos\theta + \Delta\bar{\phi}_y\sin\theta)\rho - (\beta + \frac{i\omega\rho_M}{\beta})e^{-i\omega\tau}\Delta\bar{\phi}(u,v)\Big]\frac{1}{4\pi\rho^2} \qquad (28)$$

As this function is finite and continuous for $0 \leq \rho \leq \rho_S$, we may again employ the numerical quadrature procedure described. As in the previous subcase, the application is made by using the subdivisions of Fig. 3.

The term E which is evaluated in closed form is finally defined by

$$E = \lim_{z^n \to 0} \int_0^{2\pi} d\theta \int_0^{\rho_S} \Big[\beta\Delta\bar{\phi} + ((\beta\Delta\bar{\phi}_x - \frac{i\omega}{\beta}\Delta\bar{\phi})\cos\theta + \Delta\bar{\phi}_y\sin\theta)\rho\Big](-\rho^2 + 2B(z^n)^2)\frac{\rho\,d\rho}{4\pi R^5} \qquad (29)$$

The evaluation is performed by decomposing the outer integral into subintegrals over the four triangles which are formed by the rays through the corners of S_n+W_n. Assuming that the triangle in Fig. 2 represents the r^{th} of these triangles, we may define a unit vector $\underline{e}$ along the outer edge as

$$\underline{e} = (e_x,e_y) = (\underline{\bar{x}}_3^n - \underline{\bar{x}}_2^n)/|\underline{\bar{x}}_3^n - \underline{\bar{x}}_2^n| \qquad (30)$$

Defining in addition a normal vector $\underline{n}$ by $\underline{n} = (e_y,-e_x)$, we may put

$$D = (\underline{\bar{x}}_2^n - \underline{\bar{x}}^n)\cdot\underline{n} \qquad (31)$$

$$t_2 = (\underline{\bar{x}}_2^n - \underline{\bar{x}}^n)\cdot\underline{e} \qquad t_3 = (\underline{\bar{x}}_3^n - \underline{\bar{x}}^n)\cdot\underline{e} \qquad (32)$$

$$\rho_2 = |\underline{\bar{x}}_2^n - \underline{\bar{x}}^n| \qquad \rho_3 = |\underline{\bar{x}}_3^n - \underline{\bar{x}}^n| \qquad (33)$$

$$B_1 = (\beta\Delta\bar{\phi}_x - \frac{i\omega}{\beta}\Delta\bar{\phi})e_y - \Delta\bar{\phi}_y e_x \qquad (34)$$

and

$$B_2 = (\beta\Delta\tilde{\rho}_x - \frac{i\omega}{\beta}\Delta\tilde{\rho})e_x - \Delta\tilde{\rho}_y e_y \quad (35)$$

By means of these quantities the final formula for E may be written

$$E = \frac{1}{4\pi}\sum_{r=1}^{4}(\beta\Delta\tilde{\rho}I_0 + B_1 I_1 + B_2 I_2) \quad (36)$$

where

$$I_0 = (t_3/\rho_3 - t_2/\rho_2)/D \quad (37)$$

$$I_1 = -(1+\ln\rho_3)t_3/\rho_3 + (1+\ln\rho_2)t_2/\rho_2 + \tfrac{1}{2}\ln(\rho_3+t_3)(\rho_2-t_2)/(\rho_2+t_2)(\rho_3-t_3) \quad (38)$$

and

$$I_1 = D(1+\ln\rho_3)/\rho_3 - D(1+\ln\rho_2)/\rho_2 \quad (39)$$

For practical applications of the quadrature formula (18) one has to choose suitable values for the subinterval numbers i_S and j_S. This choice is made indirectly by means of the formulas

$$i_S = P_1 + \mathrm{INT}((\rho_S-\rho_I)(P_2+P_3\omega(1+M\cos\theta)/B)) \quad (40)$$

and

$$j_S = P_4 + \mathrm{INT}(P_5|\theta_S-\theta_I|) \quad (41)$$

The function INT( ) is the largest integer that does not exceed the argument. As the integrand (8) varies more rapidly on rays in the downstream halfplane than on rays in the upstream halfplane, the factor $1+M\cos\theta$ which is larger in the former case than in the latter has been included. The parameters P_i are assigned values in accordance with the following relations

$$P_i = \begin{cases} D_{i,n} & (x^n,y^n) \text{ outside } S_n+W_n \\ \left.\begin{cases} Z_{i,n} & i \neq 2 \\ \dfrac{Z_{i,n}}{100|z^n|} & i = 2 \end{cases}\right\} & (x^n,y^n) \text{ within } S_n+W_n,\ z^n \neq 0 \\ S_{i,n} & (x^n,y^n) \text{ within } S_n+W_n,\ z^n = 0 \end{cases} \quad (42)$$

where $D_{i,n}$, $S_{i,n}$, and $Z_{i,n}$ represent specified input data. These need not be the same for the different surfaces.

Approximation of the potential jump

The advanced velocity potential jump $\Delta\tilde{\rho}(u,v)$ across S_n which was assumed given in the previous section is approximated by the linear combination

$$\Delta\tilde{\rho}(u,v) \approx \sum_{\mu=1}^{\mu_S}\sum_{\nu=1}^{\nu_S} s_\mu(\xi)t_\nu(\eta)a_{\mu,\nu} + \sum_{k=1}^{k_S}\left[F_{1,k}(\xi,\eta)C_{1,k}+F_{2,k}(\xi,\eta)C_{2,k}\right] \quad (43)$$

where $s_\mu(\xi)$, $t_\nu(\eta)$, $F_{1,k}(\xi,\eta)$, and $F_{2,k}(\xi,\eta)$ are given functions.

The latter two functions are associated with the k^{th} control-surface on S_n which may be fitted with k_S control-surfaces. These functions are in essence the same functions as those defined in Ref. 1 . They shall account for the irregular behaviour of the potential jump at the leading edge and at the side edges of the control-surface. The irregularity which corresponds to the discontinuity in the given normal velocity at these edges is obtained by considering the potential that is defined by a source distribution with a corresponding discontinuity at the control-surface edges. The discontinuity can be represented approximately by means of the coefficients $C_{1,k}$ and $C_{2,k}$ which denote the amplitudes of relative translational and rotational oscillations of the k^{th} control-surface.

The functions $s_\mu(\xi)$ which represent integrals of the Birnbaum-Glauert functions are defined by

$$s_\mu(\xi) = \begin{cases} \theta(\xi) + \xi(1-\xi^2)^{\frac{1}{2}} & \mu = 1 \\ (1-\xi)(1-\xi^2)^{\frac{1}{2}} & \mu = 2 \\ V_\mu(\xi) & \mu > 2 \end{cases} \quad (44)$$

$$V_\mu(\xi) = \begin{cases} S_1(\xi) & \mu = 1 \\ \frac{1}{4}S_2(\xi) & \mu = 2 \\ \frac{-1}{2(\mu-2)}S_{\mu-2}(\xi) + \frac{1}{2\mu}S_\mu(\xi) & \mu > 2 \end{cases} \quad (45)$$

$$S_\mu(\xi) = \sin(\mu\theta(\xi)) \quad (46)$$

and

$$\theta(\xi) = \frac{\pi}{2} + \sin^{-1}\xi \quad (47)$$

The arguments ξ and η are normalized chordwise and spanwise variables. These are defined by

$$\xi = (2u - x_T^n - x_L^n)/(x_T^n - x_L^n) \quad (48)$$

and

$$\eta = v/s \quad (49)$$

where s is the span of the trapezoidal surface S_n and x_L^n and x_T^n the x^n-coordinates for the leading and trailing edge.

The spanwise factors $t_\nu(\eta)$ are chosen either as $V_\nu(\eta)$ or as $P_{\nu-1}(\eta)$ where $P_n(\eta)$ is the Legendre polynomial of order n. The first alternative is used if the outboard chord is a free side edge while the second alternative may be used if the surface S_n is joined to other surfaces at both side edges.

The definition (48) for the variable ξ which has been chosen for the reason of simplicity is not entirely satisfactory. In case of a wing consisting of two trapezoidal parts with different edge slopes, the derivative of ξ with respect to η is discontinuous at the common chord. In order to avoid such a discontinuity for a tapered symmetrical wing, a different definition was used in Ref. 1. This is implicit and reads

$$x^n = B_1+B_2\xi +(B_3+B_4\xi)\left[\varepsilon^2(1-\xi^2)^2+\eta^2\right]^{\frac{1}{2}} \qquad (50)$$

where ε is a small arbitrary parameter. Since the coefficients B_i are defined such that

$$x_L^n = B_1-B_2+(B_3-B_4)|\eta| \qquad (51)$$

and

$$x_T^n = B_1+B_2+(B_3+B_4)|\eta| \qquad (52)$$

the definition (50) is equivalent with (48) in the case of $\varepsilon = 0$. In the case of $\varepsilon \neq 0$, the formula (50) implies that the curves, for which ξ is constant, are hyperbolas. These are regular at the root chord and the discontinuity in the derivative with respect to η is thus avoided if the definition (50) is used.

As it is difficult to define regular coordinate lines in the case of a configuration consisting of several trapezoidal parts, the formula (48) has been employed in the present version of the computer program developed.

Some initial examples

The method described, which is called the Polar Coordinate Method or the PCM for short, has been programmed in Fortran for the CDC 6600 computer.

When running this program, one has to use suitable values for the quadrature parameters $D_{i,n}$, $S_{i,n}$, and $Z_{i,n}$ and for the numbers of chordwise and spanwise factors μ_S and ν_S. In principle, it should be possible to achieve high accuracy by choosing large values for these parameters, but in practice there are certain limits. The values, that can be used, are limited by the size of the central core memory and by the acceptable computer time.

It appears, however, that satisfactory accuracy can be obtained in practical cases by using rather small values for μ_S and ν_S and the quadrature parameters. This implies that the computer time will be moderate. We try to show this in a few examples for simple wings for which reliable solutions from other independent methods are available. These examples also serve as a guide for selection of values for the arbitrary parameters in new applications.

The rectangular aspect ratio 2 wing

The rectangular aspect ratio 2 wing was treated by Garner, Hewitt, and Labrujere[6] in their investigation of three different lifting-surface theories. As the three theories produced very closely agreeing values for the lift coefficient C_L and the moment coefficient C_M, we consider these values reliable and use them for comparison. Retaining only agreeing figures, we may quote the results as $C_L = 2.474$ and $C_M = -0.518$. These values are valid for unit incidence and incompressible steady flow. The moment axis is the leading edge and the reference area and the reference length are equal to the wing area and the wing chord.

In an application of the PCM to the same wing, the numbers of chordwise and spanwise factors were chosen as $\mu_S = \nu_S = 2$. This application produced the results $C_L = 2.46$ and $C_M = -0.517$ which are in close agreement with the results of Garner, Hewitt, and Labrujere. We may hence conclude that C_L and C_M for rectangular wings can be calculated by using only a few terms in the approximations to the potential jump.

The effect of varying the input values for the quadrature parameters was studied in three runs. The result of this study is that the corresponding changes in the aerodynamic coefficients are small. The results for C_L and C_M from the three runs in which the parameter sets $D_{i,2} = S_{i,1} = 2, 8, 1, 2, 4$; $4, 16, 1, 1, 2$; and $4, 16, 1, 2, 4$ were used, were found to differ by less than one unit in the third figure.

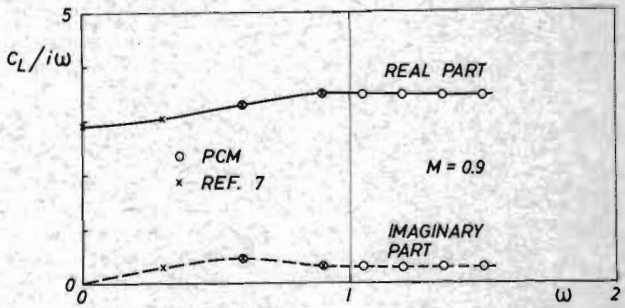

FIG. 4 LIFT COEFFICIENT FOR A RECTANGULAR A=2 WING OSCILLATING IN TRANSLATION

Considering now the case of the oscillating rectangular wing, we compare the PCM results with values from Ref. 7. These values were calculated by the method of Legendre polynomial expansion in square boxes[8]. The comparison which is made for rigid modes shows that the results from the two methods are in close agreement. This is illustrated in Fig. 4 for the lift coefficient in the case of translatory oscillations at the Mach number M = 0.9.

The Warren 12 planform

Garner, Hewitt, and Labrujere[6] treated also the swept Warren 12 planform in the investigation of the three lifting-surface theories. This wing has aspect ratio $2\sqrt{2}$, taper ratio $(3-\sqrt{2})/3 = 0.529$, and leading edge sweep angle $\tan^{-1}(1+\sqrt{2}/4) = 53.5$ degrees. The results for C_L and C_M for unit incidence in steady incompressible flow from the three theories are slightly different, but they do not deviate by more than 0.01 from the values 2.76 and -3.12 respectively. The moment coefficient is referred to the mean chord and the apex in this case.

The PCM was applied to the Warren 12 planform for the parameter values $\mu_S = \nu_S = 4$ and $D_{i,2} = S_{i,1} = 2, 8, 1, 2, 4$. The results of the application which read $C_L = 2.79$ and $C_M = -3.10$ are seen to agree satisfactorily with those of Garner, Hewitt, and Labrujere.

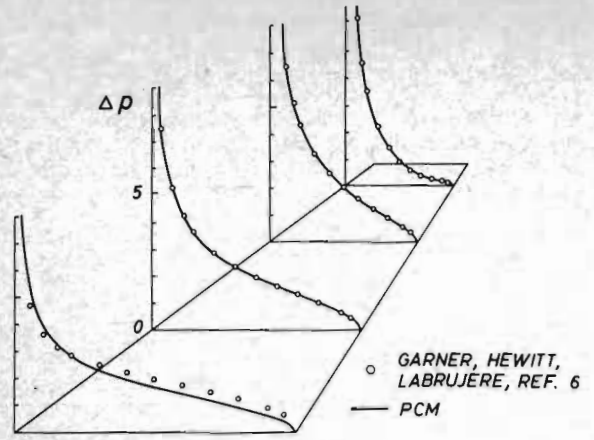

FIG. 5 DIFFERENTIAL PRESSURE ACROSS THE WARREN 12 PLANFORM. M = 0

The differences between the two solutions for the aerodynamic coefficients which amount to about 1 per cent correspond to a difference between the lift distributions produced by the two methods. From Fig. 5 we see that the two results for the lift distribution which agree very well on the outboard part of the airfoil are slightly different at the root chord. This difference may be attributed partly to the use of the formula (48) for ξ which yields a discontinuity in the spanwise derivative of the approximation.

The AGARD wing E

As an example for an oscillating swept wing we consider the AGARD wing E. This has aspect ratio 2, taper ratio 0.2376, and leading edge sweep angle 60 degrees. The oscillations considered are rigid plunging oscillations and pitching oscillations about the center of the root chord. The amplitudes are L and one radian respectively and the reference quantities L and S are equal to the semispan and the wing area.

The PCM program was applied in four runs for different parameter sets. These sets and the corresponding computer times are given in Table 1 while the resulting values for the aerodynamic coefficients are given in Table 2.

Table 1 Parameter values and computer times

Run	μ_S	ν_S	$D_{i,2} = S_{i,1}$	CP-time sec.
1	4	4	2, 8, 1, 1, 2	21.1
2	4	4	4, 16, 2, 2, 4	68.3
3	6	6	4, 16, 2, 2, 4	244.6
4	6	6	2, 8, 1, 1, 2	68.7

Table 2 Aerodynamic coefficients for the AGARD wing E. M = 0.8, ω = 1.

p	Run	$A_{p,1}$ Re	$A_{p,1}$ Im	$A_{p,2}$ Re	$A_{p,2}$ Im
1	1	-0.852	2.594	2.597	2.988
	2	-0.864	2.585	2.578	2.994
	3	-0.812	2.610	2.663	2.921
	4	-0.812	2.619	2.674	2.928
2	1	-0.485	0.690	0.432	1.644
	2	-0.486	0.686	0.427	1.643
	3	-0.502	0.715	0.470	1.693
	4	-0.503	0.717	0.473	1.696

It is seen from the table that the effect of varying the quadrature parameters is small while that of increasing the number of terms in the approximation is slightly larger.

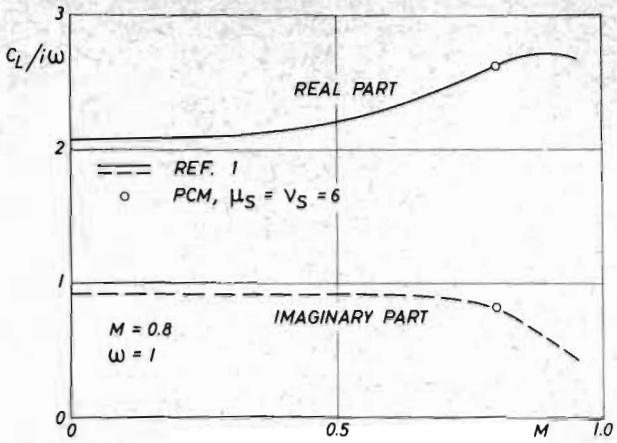

FIG. 6 LIFT COEFFICIENT FOR THE PLUNGING AGARD WING E

The values obtained for the aerodynamic coefficients in the two runs for $\mu_S = \nu_S = 6$ have been found to be in very satisfactory agreement with the results given in Ref. 1 . This agreement is illustrated by Fig. 6 in which the lift coefficient for translatory oscillations is plotted. Because of this agreement and since the independent program version that was used in Ref. 1 employs the more satisfactory definition (50) for ξ, we are inclined to believe that the results for $\mu_S = \nu_S = 6$ are accurate.

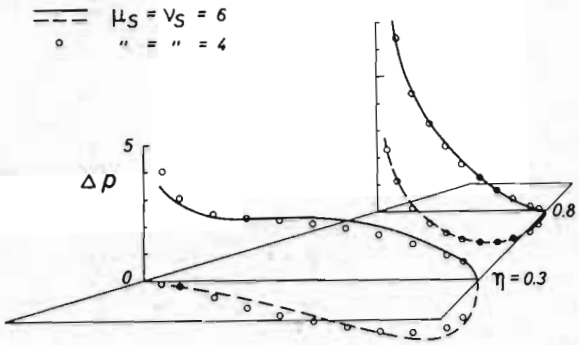

FIG. 7 DIFFERENTIAL PRESSURE ACROSS THE PLUNGING AGARD WING E. M = 0.8 , ω = 1.

By studying the lift distributions for $\mu_S = \nu_S = 4$ and $\mu_S = \nu_S = 6$ which are plotted in Fig. 7, we find again that the results for the pressure difference are more accurate on the outboard part of the airfoil than on the central part.

Application to the Viggen configuration

In the application of the PCM program to the Viggen aircraft, this has been replaced by an idealized configuration. The configuration which is shown in Fig. 8 consists of 4 pairs of trapezoidal surfaces. The main wing is represented by the surfaces S_2, S_3, S_4, S_6, S_7, and S_8 and the forward wing is represented by S_1 and S_5. The former six surfaces and the latter two lie in different parallel planes; the distance between the planes being 18.4 per cent of the semispan of the forward wing. The x- and y-coordinates of the corners of the surfaces S_n in the coordinate system of Fig. 8 are given in Table 3.

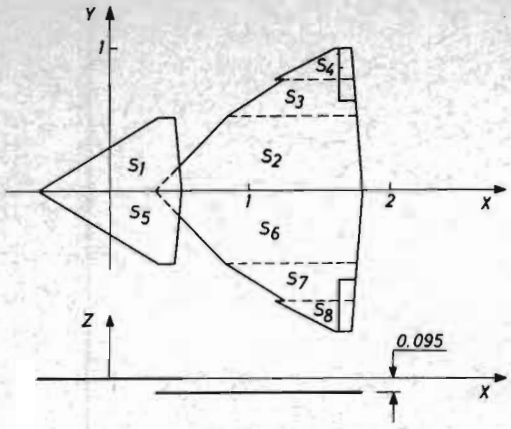

FIG. 8 IDEALIZED VIGGEN CONFIGURATION

Table 3 Coordinates of the corners of S_n

n	x-coordinates			
1	0.4664	0.3445	-0.5162	0.5162
2	1.7753	0.8381	0.3293	1.8217
3	1.7515	1.2536	0.8381	1.7753
4	1.7317	1.6159	1.1830	1.7515
	y-coordinates			
1	0.5172	0.5172	0.	0.
2	0.5172	0.5172	0.	0.
3	0.7795	0.7795	0.5172	0.5172
4	1.0000	1.0000	0.7795	0.7795

Although the PCM program is capable of treating elastic modes we limit this study to rigid modes. In addition to translation and pitch of the complete configuration, pitch of the forward wing, and translation of the main wing, we consider symmetric control-surface rotation. The leading edge which represents the axis of rotation and the inboard side edges of the control-surfaces are formed by the intersections with the planes $x = 1.6367$ and $y = \pm 0.6369$. The shape functions for the five modes may be defined as follows:

$$H_p = \begin{cases} 1 & \text{on } S_1,S_2,\ldots,S_8 & p=1 \\ x & \text{" —— " ——} & p=2 \\ \begin{cases} x+0.5162 & \text{" } S_1,S_5 \\ 0 & \text{" } S_2,S_3,S_4,S_6,S_7,S_8 \end{cases} & & p=3 \\ \begin{cases} 1 & \text{" —— " ——} \\ 0 & \text{" } S_1,S_5 \end{cases} & & p=4 \\ \begin{cases} x-1.6367 & \text{" the control-surfaces} \\ 0 & \text{off —— " ——} \end{cases} & & p=5 \end{cases}$$

The isolated main wing

As the upwash at some distance ahead of a wing is small, the interference lift on the forward wing due to deflections of the outboard or downstream part of the main wing is also small. The elements in the aerodynamic coefficient matrix, that correspond to oscillations of the control-surfaces, can thus be calculated by treating the main wing alone.

Another reason for considering the isolated main wing is the need for determining suitable values for the quadrature parameters in a simple study. The PCM program has therefore been applied for steady flow to the isolated main wing in four runs for different parameter sets:

Run 1: $D_{i,n} = 2, 16, 1, 1, 2$
$S_{i,n} = 2, 8, 1, 1, 2$

Run 2: $D_{i,n} = 2, 30, 1, 1, 2$
$S_{i,n} = 2, 8, 1, 1, 2$

Run 3: $D_{i,n} = 2, 16, 1, 1, 4$
$S_{i,n} = 2, 8, 1, 1, 2$

Run 4: $D_{i,n} = 2, 16, 1, 1, 2$
$S_{i,n} = 2, 16, 1, 1, 2$

It is possible to use different sets of parameter values for the different surfaces, but this capability has not been utilized here. The number of chordwise and spanwise factors were chosen as $(\mu_S,\nu_S) = (3,4)$, $(3,3)$, and $(3,3)$ for the three parts of each wing half.

Table 4 Lift and moment coefficient for the main wing at unit incidence in steady flow. $M = 0.9$.

Run	C_L	C_M
1	3.348	-0.053
2	3.299	-0.059
3	3.347	-0.054
4	3.348	-0.054

The results for the lift and moment coefficient are given in Table 4. It is seen from this table that the effect on C_L and C_M of the quadrature parameter variation is not large. For moderate demands on accuracy, it therefore seems satifactory to use any of the four sets.

Lift distributions and aerodynamic coefficients for oscillations in the control-surface mode have been calculated by using the parameter sets employed in the fourth run. In addition, four pairs of functions $F_{1,k}$ and $F_{2,k}$ corresponding to 2 control-surface parts for each of the surfaces S_3 and S_4 were considered in the second summation in Eq. (43) and the coefficients $C_{1,k}$ and $C_{2,k}$ for these parts were put equal to 0 and 1 respectively. The results for the aerodynamic coefficients are given in column 5 of Table 5 where results for the remaining four modes are also collected. In these calculations the central processor time for a run for one frequency value varied from 68 seconds for $\omega = 0$ to 88 seconds for $\omega = 1.067$.

As illustrations of the results we show the lift distribution and the lift coefficient for the control-surface deflection considered and steady flow in Fig. 9 and 10 respectively. The finite peak that is exhibited by the curves in Fig. 9 corresponds to the small but non-zero value that was used for the arbitrary parameter that is involved in the special functions $F_{1,k}$ and $F_{2,k}$. From Fig. 10 is further seen that the PCM results for C_L agree very well with results from a program based on the Vortex Lattice Theory[8] and also that the two theoretical solutions do not deviate too much from the experimental result.

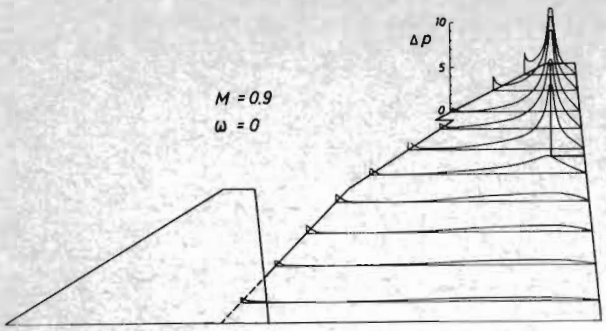

FIG. 9 LIFT DISTRIBUTION DUE TO UNIT CONTROL-SURFACE ROTATION

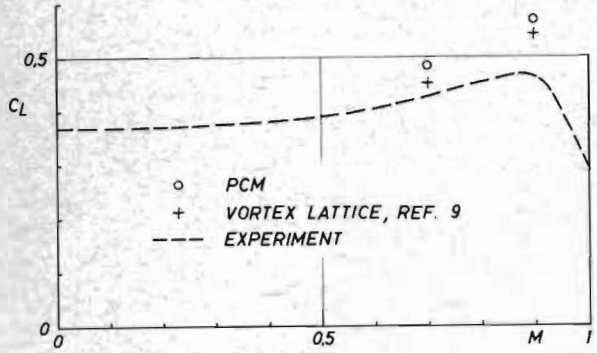

FIG. 10 LIFT COEFFICIENT FOR UNIT CONTROL-SURFACE ROTATION

Interference effects

Turning now to the complete configuration we first make a special test. We consider the normal velocity that is obtained at points on the main wing for a given potential jump across the forward wing and its wake. In the steady case the jump across the wake is independent of the streamwise coordinate and the flow at a station sufficiently far downstream is therefore two-dimensional. We utilize this fact in a check for verifying the accuracy of the three-dimensional numerical quadrature procedure.

We consider the first three functions in the approximation to the potential jump across the forward wing. The corresponding potential jumps across the wake of the forward wing are illustrated in the small figure at the top of Fig. 11. The corresponding normal velocities can easily be calculated by means of the Chebyshev functions. The results of such a two-dimensional calculation for points on the plane of the main wing are represented by the curves in the main figure.

The circles in the same figure represent normal velocity values calculated by the PCM program at points on a line close to the trailing edge of the main wing. Calculations were made both for M = 0.7 and M = 0.9, but the results do not differ significantly.

At the streamwise station considered and for the Mach numbers mentioned the flow is nearly two-dimensional. Therefore, it is very gratifying that there is such a close agreement between the results from the two-dimensional theory and from the PCM program. The figure shows in particular that the agreement is close for the third function for which the deviation from two-dimensional flow is smallest and the demand on the quadrature procedure highest.

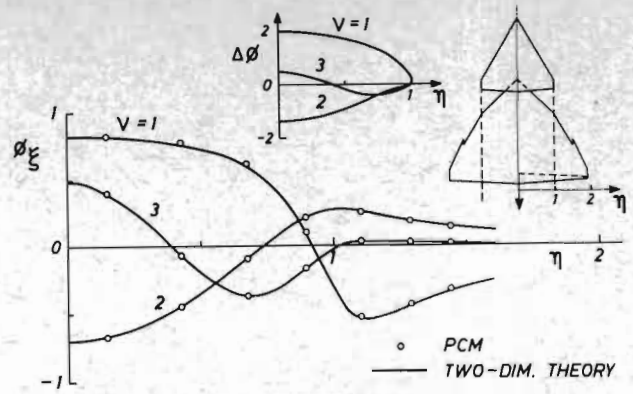

FIG. 11 NORMAL VELOCITY ON THE PLANE OF THE MAIN WING INDUCED BY A POTENTIAL JUMP ACROSS THE FORWARD WING AND ITS WAKE

The agreement confirms that the parameter values employed in the PCM calculation are sufficient. These values read

$$D_{i,n} = 2, 16, 1, 1, 2 \qquad n = 1, 5$$

and

$$Z_{i,1} = 2, 3, 1, 1, 2$$

By separate runs like those for the isolated main wing, it has further been found that the values

$$D_{i,5} = 2, 16, 1, 1, 2$$

and

$$S_{i,1} = 2, 16, 1, 1, 2$$

seem to be satisfactory for the isolated forward wing. In the application to the complete configuration, we have therefore used these values together with the values employed in Run 4 for the isolated main wing. The number of chordwise factors in the approximations was chosen as 3 for each of the surfaces while the number of spanwise factors was chosen as 4 for S_1, S_2, S_5, and S_6 and as 3 for S_3, S_4, S_7, and S_8.

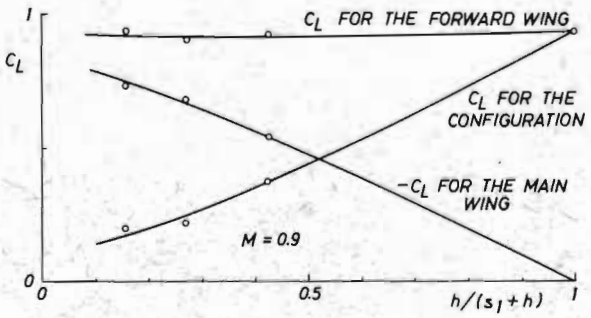

FIG. 12 LIFT ON THE CONFIGURATION AND THE TWO WINGS DUE TO UNIT PITCH OF THE FORWARD WING.

It is interesting to consider the third mode in which case the normal velocity equals unity on the forward wing and zero on the main wing. The lift coefficients for the forward wing, the main wing, and the complete configuration in steady flow have been calculated for different separations of the two wing planes. The results are shown in Fig. 12 as functions of $h/(s_1+h)$ where h is the separation and s_1 the semispan of the forward wing.

The values plotted for $h/(s_1+h) = 1$ were obtained in a run for $h/s_1 = 36.8$ in which case the interference effects may be considered to be very small. As these values were found to agree very closely with those from the runs for the isolated wings, we may regard this as a check on the proper function of the program.

Calculations have further been performed for $h/s_1 = 0.184$, 0.368, and 0.736. These runs were made for the quadrature parameter values mentioned above, but the run for $h/s_1 = 0.184$ was also repeated for $D_{i,n} = 2, 30, 1, 1, 2$; $S_{i,n} = 2, 30, 1, 1, 2$; and $Z_{i,n} = 2, 4, 1, 1, 2$. The effect of the increase in the parameters was insignificant, however. For this reason and because of the comparison in Fig. 11, which indicates that the calculation of the downwash due to the potential jump across the forward wing and its wake should be accurate, we believe that the results in Fig. 12 are rather satisfactory.

It is seen from the figure that the interference lift on the main wing increases as the separation h of the two wing planes decreases while the lift on the forward wing seems to be nearly independent of h. The interference lift on the main wing which is opposite in direction to the direct lift on the forward wing almost cancels the latter as h goes to zero.

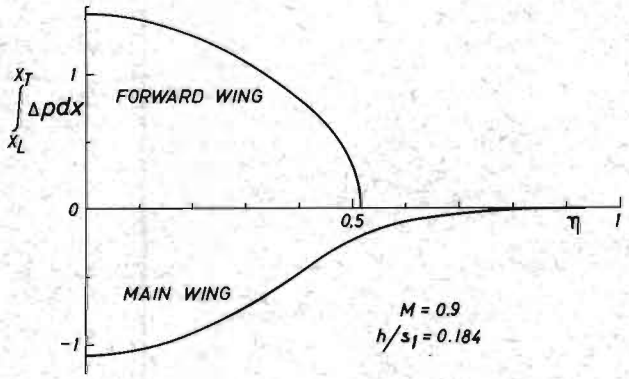

FIG. 13 LIFT ON UNIT SPAN ON THE FORWARD WING AND THE MAIN WING DUE TO UNIT INCIDENCE OF THE FORMER

From Fig. 13 in which the spanwise distribution of the load on the forward wing and the main wing are plotted for M = 0.9 and $h/s_1 = 0.184$ we further see that the interference load on the outboard part of the main wing is very small. For this reason and as the interference lift on the forward wing due to deflections of the outboard part of the main wing is also very small, it doe not appear likely that flutter can occur because of aerodynamic coupling between the two wings.

Results for the oscillating configuration

Continued applications of the PCM program to the Viggen configuration have been made in the unsteady case with a view to calculate aerodynamic coefficients for the five modes defined. The program has been run for the Mach number M = 0.9 and for three non-zero values of the reduced frequency ω. The quadrature parameter values were chosen as $D_{i,n} = 2, 16, 1, 1, 2$; $S_{i,n} = 2, 16, 1, 1, 2$; and $Z_{i,n} = 2, 3, 1, 1, 2$ which implies that the values employed in the steady case were retained. The number of spanwise factors in the approximations was also retained but the number of chordwise factors for the main wing was increased. The number was increased to four for each part of this wing. The increase is desirable, for the appearing chordwise variations are becoming more pronounced as the frequency increases.

Table 5 Aerodynamic coefficients $A_{p,q}$ for the Viggen configuration. M = 0.9 .

ω	p \ q	1 Re	1 Im	2 Re	2 Im	3 Re	3 Im	4 Re	4 Im	5 Re	5 Im
0.	1	0	0	5.977	0	0.336	0	0	0	0.9429	0
	2	0	0	5.169	0	-0.901	0	0	0	1.4535	0
	3	0	0	0.905	0	0.798	0	0	0	0.	0
	4	0	0	4.349	0	-1.146	0	0	0	0.9429	0
	5									0.0056	0
0.355	1	-0.234	2.128	6.024	3.969	0.241	0.549	-0.083	2.000	0.9158	-0.1987
	2	-0.347	1.880	5.113	4.851	-1.010	-0.005	-0.256	2.210	1.4631	-0.2222
	3	-0.018	0.306	0.889	0.218	0.798	0.465	0.033	0.012	0.	0.
	4	-0.219	1.578	4.426	5.704	-1.255	-0.126	-0.178	1.991	0.9158	-0.1987
	5									0.0058	0.0019
0.711	1	-0.940	4.500	6.477	8.005	-0.020	1.217	-0.311	4.158	0.7458	-0.2888
	2	-1.320	4.165	5.406	10.000	-1.329	0.119	-0.883	4.815	1.2762	-0.3815
	3	-0.141	0.622	0.861	0.545	0.816	0.919	0.020	-0.025	0.	0.
	4	-0.782	3.381	4.886	7.319	-1.571	-0.100	-0.330	4.188	0.7458	-0.2888
	5									0.0061	0.0037
1.067	1	-1.844	7.101	7.084	11.342	-0.309	2.130	-0.455	6.266	0.5668	-0.2964
	2	-2.402	6.930	6.220	14.432	-1.679	0.568	-1.294	7.643	1.0362	-0.4496
	3	-0.293	0.958	0.924	0.791	0.793	1.559	0.008	-0.038	0.	0.
	4	-1.508	5.411	5.405	13.561	-1.845	0.219	-0.436	6.311	0.5668	-0.2694
	5									0.0061	0.0051

The values calculated for the aerodynamic coefficients in these runs are given in column 1 to 4 of Table 5; column 5 contains the results from the runs for the isolated main wing. The reference length that applies to the values in the table and to the values of the reduced frequency is equal to the semispan of the main wing while the reference area is the square of this length.

The central processor time for the four runs for the oscillating configuration varies from 92 seconds for $\omega = 0$ to 122 seconds for $\omega = 1.067$.

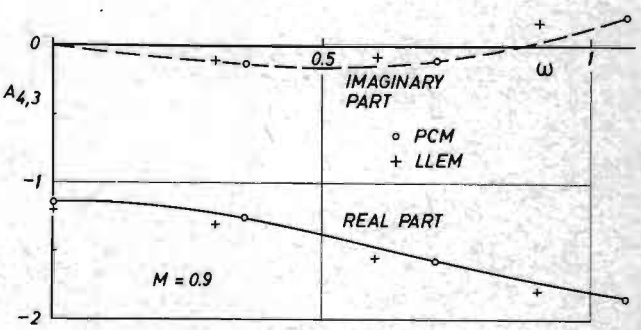

FIG. 14 LIFT ON THE MAIN WING DUE TO PITCHING OSCILLATIONS OF THE FORWARD WING

Comparison with results of the Lifting Line Element Method

The Lifting Line Element Method or the LLEM for short is a generalization for unsteady flow of the Vortex Lattice Theory[9]. The LLEM utilizes complex cross-flow representation[5] and Legendre functions of the second kind[4]. Results from applications to the Viggen configuration of the LLEM which is much like the independently developed Doublet Lattice Method[10] were presented in Ref. 4.

We also show some early LLEM results together with corresponding PCM results in Fig. 14. This figure illustrates the lift on the main wing due to pitching oscillations of the forward wing about its apex. The LLEM results which were obtained by using only 9 elements on each half of the forward wing and 27 elements on each half of the main wing correspond to a separation between the wing planes

that is 25 per cent of the semispan of the forward wing while the PCM results correspond to a separation of 18.4 per cent. It is apparent, however, that even if a correction for the difference in separation is made, the two solutions exhibit a good agreement with regard to the small number of elements in the LLEM-solution.

It may further be mentioned that the calculation of the interference lift on the main wing due to deflections of the forward wing seems to represent a tricky problem. The solutions obtained by the LLEM and the Vortex Lattice Theory in the steady case have been found to be sensitive to the arrangement of vortices and the solutions by the PCM program appear sensitive to the number of chordwise and spanwise factors in the approximations. Further studies are therefore required if solutions with increased accuracy are needed.

Conclusions

A Fortran program based on the Polar Coordinate Method for calculation of aerodynamic forces on oscillating wing configurations with control-surfaces in subsonic flow has been investigated. Its practical usefulness has been studied in applications to the Viggen configuration and its numerical accuracy has been investigated through parameter variations and by comparisons with certain reliable results of other methods.

The investigation indicates that the program works properly and that it produces reliable results if appropriate values for the arbitrary parameters involved are supplied. For practical applications it seems sufficient to use moderate values for these parameters which implies moderate computer times and costs.

For large values of the parameters, the program probably yields high accuracy which may be utilized for comparisons.

References

1. Stark, V. J. E.,"A subsonic oscillating-surface theory for wings with partial-span controls", AIAA Paper No. 72-61, Jan., 1972.
2. Stark, V. J. E.,"Application of the Polar Coordinate Method to oscillating wing configurations", Saab Technical Note, TN 69, Dec., 1973.
3. Stark, V. J. E.,"The Tangent Plane Method and polar coordinates -- A new approach in lifting-surface theory", AIAA Paper No. 70-78, Jan. 1970.
4. Landahl, M. T. and Stark, V. J. E., "Numerical lifting-surface Theory -- Problems and progress", AIAA J., Vol. 6, No. 11, Nov. 1968, pp. 2049-2060.
5. Stark, V. J. E.,"Use of complex cross-flow representation in nonplanar oscillating-surface theory", AIAA J., Vol. 6, No. 8, Aug. 1968, pp. 1535-1540.
6. Garner, H. C., Hewitt, B. L., and Labrujere, T. E.,"Comparison of three methods for the evaluation of subsonic lifting-surface theory", N. L. R. TR G.65, 1968.
7. Stark, V. J. E.,"Applications at M=1 of a method for solving the subsonic problem of the oscillating finite wing with the aid of high-speed digital computers", Proceedings of the International Union of Theoretical and Applied Mechanics Symposium Transsonicum, Aachen (1962) Springer-Verlag, Berlin-Göttingen-Heidelberg, 1964, pp. 440-455.
8. Stark, V. J. E.,"A method for solving the subsonic problem of the oscillating finite wing with the aid of high-speed digital computers," Saab Aircraft Co., Linköping, TN 41, Dec. 1958.
9. Hedman, S.,"Vortex lattice method for calculation of quasi steady state loadings on thin elastic wings in subsonic flow", Rept. 105, 1966, Flygtekniska Försöksanstalten (FFA), Stockholm.
10. Albano, E., and Rodden, W. P., "A doublet lattice method for calculating lift distributions on oscillating surfaces in subsonic flows", AIAA J., Vol. 7, No. 2, Feb. 1969, pp. 279-285.

D I S C U S S I O N

A. Das (DFVLR, Braunschweig, Germany): As one of the main results in your paper, the lift induced on the rear wing due to oscillations of the front wing in pitching motion has been shown. It comes out that the contribution to the lift appears mainly as a real part in the whole frequency range, while the imaginary part is quite negligible.

This property may be attributed to the particular configuration used in the example; - for a different wing spacing or wing geometry the imaginary part may play a significant role. In order to study this effect and give more insight into this problem, some parametric changes may be taken up.

V.J.E. Stark: For other tandem configurations, a time delay roughly equal to the distance between the two wings divided by the flight speed may appear. Results from other examples support this statement.